Journal of Energy Chemistry 72 (2022) 158–165

Contents lists available at ScienceDirect

Journal of Energy Chemistry

journal homepage: www.elsevier.com/locate/jechem

http://www.journals.elsevier.com/journal-of-energy-chemistry/

Thermal safety of dendritic lithium against non-aqueous electrolyte in pouch-type lithium metal batteries

Feng-Ni Jiang [a,b], Shi-Jie Yang [d], Xin-Bing Cheng [b,c,*], Peng Shi [b], Jun-Fan Ding [d], Xiang Chen [b], Hong Yuan [d], Lei Liu [a,*], Jia-Qi Huang [d], Qiang Zhang [b,*]

[a] College of Chemistry and Chemical Engineering, Taiyuan University of Technology, Taiyuan 030024, Shanxi, China
[b] Beijing Key Laboratory of Green Chemical Reaction Engineering and Technology, Department of Chemical Engineering, Tsinghua University, Beijing 100084, China
[c] Key Laboratory of Energy Thermal Conversion and Control of Ministry of Education, School of Energy and Environment, Southeast University, Nanjing 211189, Jiangsu, China
[d] Advanced Research Institute of Multidisciplinary Science, Beijing Institute of Technology, Beijing 100081, China

ARTICLE INFO

Article history:
Received 17 March 2022
Revised 26 April 2022
Accepted 4 May 2022
Available online 10 May 2022

Keywords:
Pouch-type cell
Battery safety
Lithium metal anode
Lithium dendrite growth
Thermal runaway

ABSTRACT

A quantitative relationship between safety issues and dendritic lithium (Li) has been rarely investigated yet. Herein the thermal stability of Li deposits with distinct surface area against non-aqueous electrolyte in pouch-type Li metal batteries is probed. The thermal runaway temperatures of Li metal batteries obtained by accelerating rate calorimeter are reduced from 211 °C for Li foil to 111 °C for cycled Li. The initial exothermic temperature is reduced from 194 °C for routine Li foil to 142 °C for 49.5 $m^2 g^{-1}$ dendrite. Li with different specific surface areas can regulate the reaction routes during the temperature range from 50 to 300 °C. The mass percent of Li foil and highly dendritic Li reacting with ethylene carbonate is higher than that of moderately dendritic Li. This contribution can strengthen the understanding of the thermal runaway mechanism and shed fresh light on the rational design of safe Li metal batteries.

1. Introduction

The demand on high-capacity rechargeable batteries applied in electric vehicles and large-scale stationary energy storage systems is increasing rapidly [1–6]. The lithium metal batteries (LMBs) have been strongly regarded as the most promising next-generation batteries due to their high theoretical specific capacity (3860 mAh g^{-1}) and the low potential (−3.040 V vs. the standard hydrogen electrode) of Li metal anode [7–10]. However, the use of Li metal is confronted with many serious problems induced by dendritic Li growth, such as low Coulombic efficiency (CE), short lifespan, and poor safety performance. During the past ten years, strategies including electrolyte additives [11,12], artificial solid-electrolyte interphase (SEI) [13–15], solid-state electrolytes [16–18], and 3D host design [19–21] have been proposed to improve the CE and cycling lifespan, while the understandings on the failure mechanism involving the safety performance of LMBs have been few investigated yet [22–26]. In the late 1980s, cylindrical-type cells with Li metal anode have been commercialized for the first time. However, they were recalled due to the potential fire incidents and explosions [27,28]. Therefore, safety issues are the most important challenges in the practical applications of LMBs.

Thermal runaway resulting from the mismatch between heat production and dissipation is the intrinsic reason for the safety challenges of working batteries [29,30]. Abuse conditions including mechanical, electronic, and thermal abuses can trigger serious safety risks and even the thermal runaway of batteries accompanied by the soaring temperature, toxic gas, and smoke [31–34]. In addition to the internal short-circuit initiated from the collapse of separators [35–37] and the active oxygen released from the decomposition of the cathode [38], the Li deposits on the anode [39] are considered as one of the most frequent detonators that determine the thermal runaway of Li ion batteries (LIBs). The reaction between the intercalated Li and the electrolyte is one of the main exothermal reactions leading to the thermal runaway of LIBs [40–42]. For LMBs, Li metal anode tends to form Li dendrites with high specific surface area, which will further strengthen exothermic reactions [43–46]. Therefore, the reactions between electrolyte and Li metal anode should be comprehensively explored.

To date, the exothermic chain reactions resulting in the thermal runaway of LMBs are few touched. Li metal is thermodynamically unstable against organic solvents. It can be corroded continuously

* Corresponding authors.
E-mail addresses: chengxb@seu.edu.cn (X.-B. Cheng), liulei@tyut.edu.cn (L. Liu), zhang-qiang@mails.tsinghua.edu.cn (Q. Zhang).

https://doi.org/10.1016/j.jechem.2022.05.005

by solvents and large amounts of heat is generated as the SEI is repeatedly damaged and constructed [47,48]. In addition, Li deposits during cycling influenced by the different operation conditions are highly dendritic [49–52]. Consequently, Li deposits with high specific surface areas can potentially lead to the high reactivity with the electrolyte [53]. However, the roles of Li dendrites with high specific surface areas on the safety of batteries are an open field. Therefore, it is necessary to analyze the kinetic process between Li dendrite and electrolyte, and reveal their roles on the safety issues of LMBs.

In this contribution, the underlying correlation between the thermal safety of LMBs and Li dendrite is quantitatively explored by accelerating rate calorimeter (ARC). It is displayed by the different thermal features including the self-heating temperature (T_1) and thermal runaway temperature (T_2) of LMBs with the same cathode and different anodes. The exothermic reactions between Li dendrites with different specific surface areas and lithium hexafluorophosphate ($LiPF_6$)-ethylene carbonate (EC)/diethyl carbonate (DEC) electrolyte are quantitatively investigated by differential scanning calorimeter (DSC). The features of exothermic peaks, i.e., the peak positions, are utilized to figure out the negative influence of the pulverization of Li anode on the thermal safety of LMBs. This contribution quantifies the thermal stability between dendritic Li and routine aqueous electrolytes, which affords a rational and clear basis from the battery safety viewpoint to regulate the uniform deposition of Li metal during the cycling of LMBs. In addition, the composition of electrolyte is demonstrated to have effects on the thermal safety of LMBs as well. Therefore, adjusting the ratio of different solvents in electrolytes is thought to be a simple potential strategy to improve the safety performance of LMBs.

2. Experimental

2.1. Materials

1.0 M $LiPF_6$-EC/DEC (1:1 in volume) electrolyte, $LiPF_6$, EC, DEC, and 1,2-dimethoxyethane (DME) solvents were obtained from Suzhou Duoduo Chemical Technology Co., Ltd. $LiNi_{0.5}Co_{0.2}Mn_{0.3}O_2$ (NCM523) cathode with the area capacity of 4 mAh cm^{-2} was purchased from Guangdong Canrd New Energy Technology Co., Ltd. Lithium (Li) metal (50 and 600 μm) was obtained from China Energy Lithium Co., Ltd. Celgard 2325 polypropylene-polyethylene-polypropylene (PP-PE-PP) separator was acquired from Asahi Kasei Techno system Co., Ltd. Hydrochloric acid (HCl) and ethyl alcohol were gained from Shanghai Titan Technology Co., Ltd. Acetone was obtained from Sinopharm Chemical Reagent Co., Ltd.

2.2. Assembly of pouch-type batteries

To probe the effect of Li dendrites on the safety of Li-metal batteries, pouch-type batteries with the same cathodes and different anodes were chosen for adiabatic ARC tests (Fig. S1). All pouch-type batteries (4.0 × 7.0 cm^2) were fabricated layer by layer with the alternation of cathodes, anodes, and separator in a dry room with a dew-point temperature of −40 °C. NCM523, Li electrodes (0.56 Ah, 10 mAh cm^{-2}) with Li foils (50 μm) rolled onto two sides of Cu plate (12 mm thick Cu plates), 4.0 g $LiPF_6$-EC/DEC (1:1 by vol.) electrolyte, and PP-PE-PP separator were used in pouch-type batteries. The 0.896 Ah Li||NCM batteries were charged at 0.32 mA cm^{-2} (0.08 C) between 2.8–4.3 V, then the charged NCM cathodes were disassembled from these batteries. The Li||Cu batteries were discharged at 10.59 mA cm^{-2} with a capacity of 0.56 Ah to obtain the Cu plates with Li deposits. Finally, two pouch-type cells with the same NCM cathodes but different anodes (Li foils and deposited Li) were fabricated for the ARC tests. Considering the porosity of deposited Li encapsulating electrolyte during the disassembling process of cells, the mass of electrolyte for cells with Li foil (4 g) is a bit higher than that for cells with deposited Li (3.5 g).

2.3. Fabrication of Li deposits with different specific surface areas

The electrolytic cell with copper (Cu) working electrode and Li counter electrode was utilized to obtain the Li deposits with different specific surface areas. The Cu foil was soaked in 0.10 mol L^{-1} HCl for 10 min and then washed with acetone and ethanol 3 times in turn to eliminate the impurities on the Cu foil. Then the hole punch was used to cut the Cu foil into a circular electrode with a diameter of 19 mm. The one side of the Cu working electrode was covered by Kaption adhesive tape to achieve the single-side deposition of Li metal. The Li plate with a diameter of 16 mm and a thickness of 600 μm was used as the counter electrode. The electrolytic cell with Cu and Li electrode was fabricated in an Ar-filled glove box (H_2O < 0.1 ppm, O_2 < 0.1 ppm) and 25 mL $LiPF_6$-EC/DEC (1:1 by vol.) electrolyte was added with the immersion of these two electrodes. Finally, different current densities including 0.07, 0.16, 0.35, 0.71, 1.59, and 10.59 mA cm^{-2} and a constant depositing capacity (3.18 mAh cm^{-2}) were applied to acquire the Li deposits with a series of specific surface areas.

2.4. Investigations on thermal stability

DSC was used to assess the influence of Li dendrites on the safety of batteries at material levels. The Li deposits with different surface areas and the $LiPF_6$-EC/DEC electrolyte were sealed into crucibles in glove boxes. Then they were transferred into the DSC (Q2000 TA) measurement with a temperature procedure of 10 °C min^{-1} from 30 to 300 °C under Ar atmosphere. It is worth noting that the heat flow of DSC was calculated based on the mass of Li metal and the DSC tests for each sample were repeated at least twice for the reliability of the experiment.

The safety performance of pouch-type batteries with different anodes was tested by ARC which was produced by thermal hazard technology and was conducted in a heat-wait-seek (HWS) procedure. A heating increment of 10 °C is adopted from 40 °C with a waiting time of 30 min. Then the self-heat rate of batteries is detected and compared with 0.02 °C min^{-1}. If it exceeds 0.02 °C min^{-1}, the temperature is defined as T_1 and ARC switches into adiabatic mode. Then the onset temperature of the thermal runway (T_2) is obtained when the temperature rising rate of battery reaches 1 °C s^{-1}. Otherwise, the ARC would repeat the HWS procedure until the thermal runaway of batteries or reaching a preset temperature limit of 400 °C. In addition, the real-time open-circuit voltage (OCV) of batteries was also monitored during the ARC test.

2.5. Characterization of Li deposition

The surface morphologies of the Li deposits were obtained with a JSM 7401F (JEOL Ltd., Tokyo, Japan) scanning electron microscopy (SEM). The Cu plates with Li deposits were washed by DME solvent before the SEM test. The mass of Li metal containing on the Cu plate was measured by the gas chromatography (Agilent 7890A GC) and the experiment was repeated at least twice for much reliable results (Fig. S2). The Cu plate with Li deposits was placed into the head space bottle which was usually used to collect gas for the GC analysis. Then excess ethyl alcohol (0.5 mL) was injected into the bottle to react with Li metal for a long time (15 min) until bubbles generated from the reaction were not formed and the meteorological product (H_2) of the reaction was restricted in the head space bottle. The 10 mL injection syringe was utilized to transfer

the resultant gas into the GC system for measuring the amount of H_2. Finally, the content of Li metal was calculated based on the chemical reaction [54].

$$2Li + 2C_2H_5OH \rightarrow 2C_2H_5OLi + H_2\uparrow$$

2.6. Calculation of the specific surface area of deposited Li obtained at different current densities

Considering the features of SEI including porosity and thermal instability, the specific surface areas of Li deposits are preferred to be calculated according to their mass rather than Ar desorption process. To obtain the specific surface area of Li dendrites, two hypotheses are made, i.e., the cross-section of Li dendrites is circular and the Li dendrites distribute evenly and tightly on the Cu plate (Fig. S3). Then the specific surface area of Li dendrites can be calculated through the following steps.

(1) The volume of total Li deposits (V_{Li}) is calculated by dividing metallic Li mass by its density.

$$V_{Li} = \frac{m_{Li}}{\rho_{Li}} \quad (1)$$

(2) As the lithium dendrites are tightly stacked on the Cu plate, the number of columnar Li (N_{Li}) can be expressed as.

$$N_{Li} = \frac{S_{Cu}}{d_{Li}^2} \quad (2)$$

(3) The volume of a single lithium dendrite (V_1) can be calculated as.

$$V_1 = \frac{V_{Li}}{N_{Li}} = \frac{m_{Li} d_{Li}^2}{\rho_{Li} S_{cu}} \quad (3)$$

(4) The length of Li dendrite (h) can be obtained by dividing the volume of a single lithium dendrite by the bottom area of the Li dendrite.

$$h = \frac{V_1}{S_{Li}} = \frac{4m_{Li}}{\rho_{Li} S_{cu} \pi} \quad (4)$$

(5) The total specific surface area of columnar Li (S) obtained at different current densities can be calculated as the following equation.

$$S = S_1 + S_2 = (S_{Li} + \pi d_{Li} h) \times N_{Li} = \frac{S_{cu}\pi}{4} + \frac{4m_{Li}}{\rho_{Li} d_{Li}} \quad (5)$$

where m_{Li} is the Li mass on the Cu electrode, ρ_{Li} is the density of Li metal, S_{Cu} represents the surface area of Cu electrode, d_{Li} is the diameter of columnar Li obtained at different current densities, S_{Li} is the bottom area of a single Li dendrite, S_1 and S_2 are the total base area and side area of column Li respectively.

2.7. Density functional theory calculations

The lowest unoccupied molecular orbital of EC and DEC molecules were calculated by density functional theory calculations, conducted in Gaussian (G09) suite of program with Becke's three-parameter hybrid method using the Lee-Yang-Parr correlation function (B3LYP) [55]. The geometrical structures and the vibrational modes were calculated at 6-311++G(d, p) level. Simultaneously, the solvation effect was considered with an universal solvation model of SMD [56]. The dielectric constant of EC and DEC is set to 89.78 and 2.81, respectively.

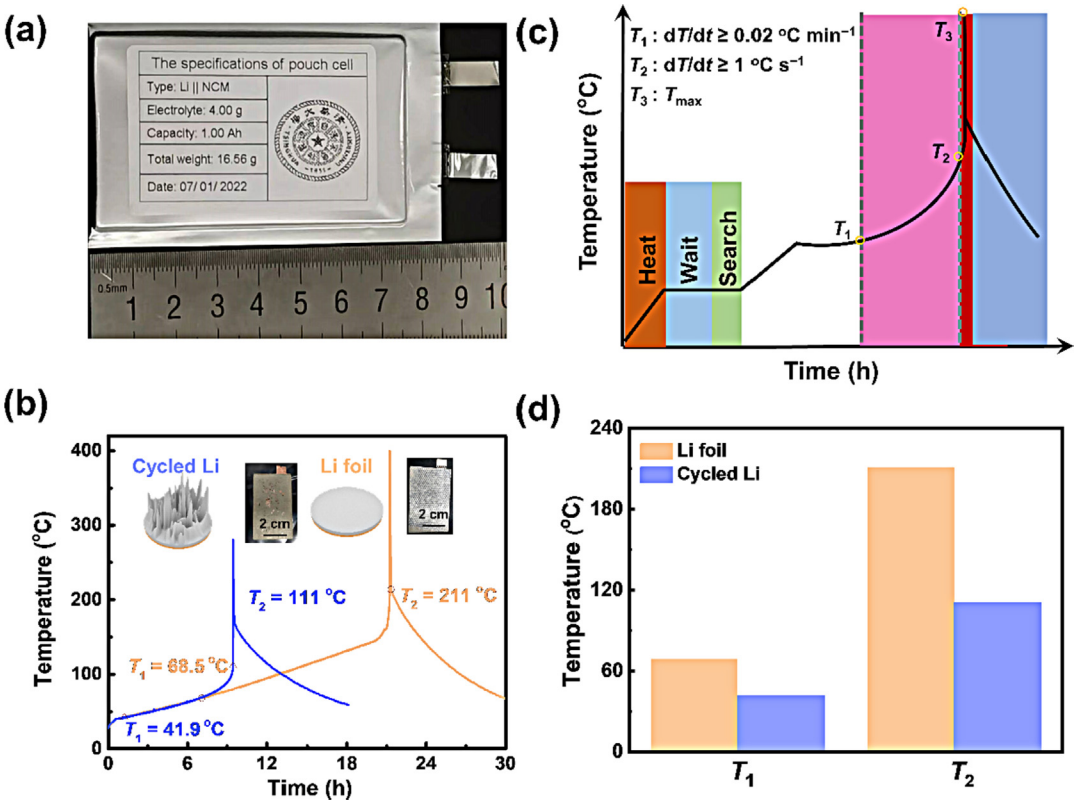

Fig. 1. Thermal runaway features of Li||NCM pouch-type cells. (a) Optical photograph of Li||NCM pouch-type cell. (b) ARC results of Li||NCM pouch-type cells with Li foil and cycled Li obtained at 10.59 mA cm^{-2} as their anodes. (c) A typical ARC test curve. The dT/dt and T_{max} are the rate of temperature rise and the highest temperature of the cell during the ARC tests respectively. (d) Comparisons of ARC results for Li||NCM cells with different Li anodes.

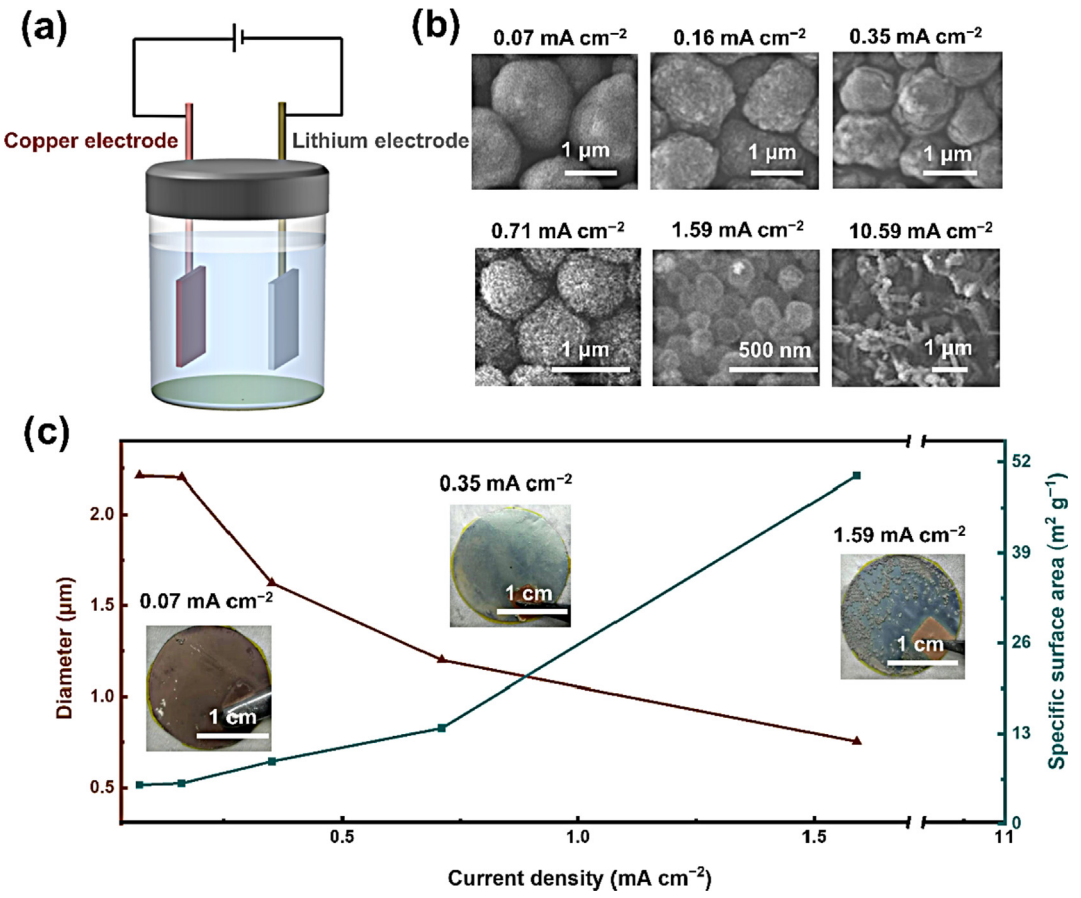

Fig. 2. Characterizations for Li deposits. (a) Schematic diagram of electrolytic cell used to obtain the Li deposits. (b) SEM images of Li deposits obtained at different current densities. (c) The dependence of the diameters and specific surface areas of Li deposits on the current densities. As the dendritic Li obtained at 10.59 mA cm^{-2} is disordered, its diameter and specific surface area are unable to be calculated. The inserts in (c) are the typical images of Li deposits obtained at different current densities.

3. Results and discussion

3.1. Thermal runaway of Li-NCM pouch-type cells

The relationship between Li dendrite with different surface areas and Coulombic efficiency, as well as the lifespan, has been widely probed [57]. However, the significance of LMBs with dendrite-free working Li metal anode during cycling has not been highlighted and demonstrated from the security standpoint until now.

The thermal runaway behaviors of Li||NCM pouch-type cells with different anodes and the same cathode were explored by adiabatic ARC to demonstrate the roles of dendritic Li on the thermal safety of practical Li metal pouch-type cells (Fig. 1a). ARC is in quasi-adiabatic condition until the appearance of thermal runaway. Therefore, it is a highly sensitive instrument to evaluate the thermal safety of batteries with comparable indexes including the two characteristic temperatures (T_1 and T_2). T_1 is the self-generated-heat temperature with a self-heating rate $\geq$ 0.02 °C min^{-1} while T_2 is a thermal-runaway temperature with a self-heating rate $\geq$ 1 °C s^{-1} (Fig. 1c). For a scientific comparison, the adopted cathode is $LiNi_{0.5}Co_{0.2}Mo_{0.3}O_2$ (NCM) obtained after once charging to 100% State of Charge (SOC), while the adopted anode is the fresh Li foil and Li deposits obtained at 10.59 mA cm^{-2}.

For LMBs with fresh Li foil as the anode, T_1 and T_2 are 68.5 and 211 °C respectively, while T_1 locates at 41.9 °C and T_2 reaches at 111 °C in the case of Li deposits as the anode (Fig. 1b and d). As demonstrated before, T_1 is caused by the decomposing of SEI, while T_2 is caused by the reactions between Li metal and the electrolyte. Therefore, cycled Li with many dendrites seriously accelerates the side reactions and deteriorates the safety performance. Besides, during the ARC tests, gas generation is obviously observed for the cell containing Li deposits with the pouch bag bulge (Fig. S4). The evolution of flammable gas is a serious problem and has a negative influence on the safety of batteries [58,59]. As a result, it is demonstrated that the drastic exothermic reactions within LMBs are further strengthened with the pulverization of Li anodes.

3.2. Li deposits with different specific surface areas

The reaction between Li metal and electrolyte is one of the main exothermic reactions during the thermal runaway of LMBs. Therefore, the thermal behavior between Li metal with different specific surface areas and 1.0 M $LiPF_6$-EC/DEC (1:1 by vol.) electrolyte was further investigated by DSC to analyze the characteristics of the reaction and propose the corresponding solutions to improve the thermal safety of LMBs. The Li deposits on the Cu plate at different current densities are obtained in a typical electrolytic cell (Fig. 2a) [60]. Uniform and dense Li deposits are achieved when the current density is below 0.71 mA cm^{-2} (Fig. 2c and Fig. S5a). A locally inhomogeneous Li deposit is observed as many bumps on Cu current collectors at the current density larger than 0.71 mA cm^{-2}. The sites with uniform Li deposits obtained at both 0.71 and 1.59 mA cm^{-2} were utilized for SEM and DSC tests (Fig. 2c and Fig. S5b). The average diameter of deposited Li columns ranges from 0.16 to 1.62 μm, decreasing with the rise of current density (Fig. 2b and c and Figs. S6 and S7), which is dominated by nuclei size and number density [61,62]. The specific surface area of

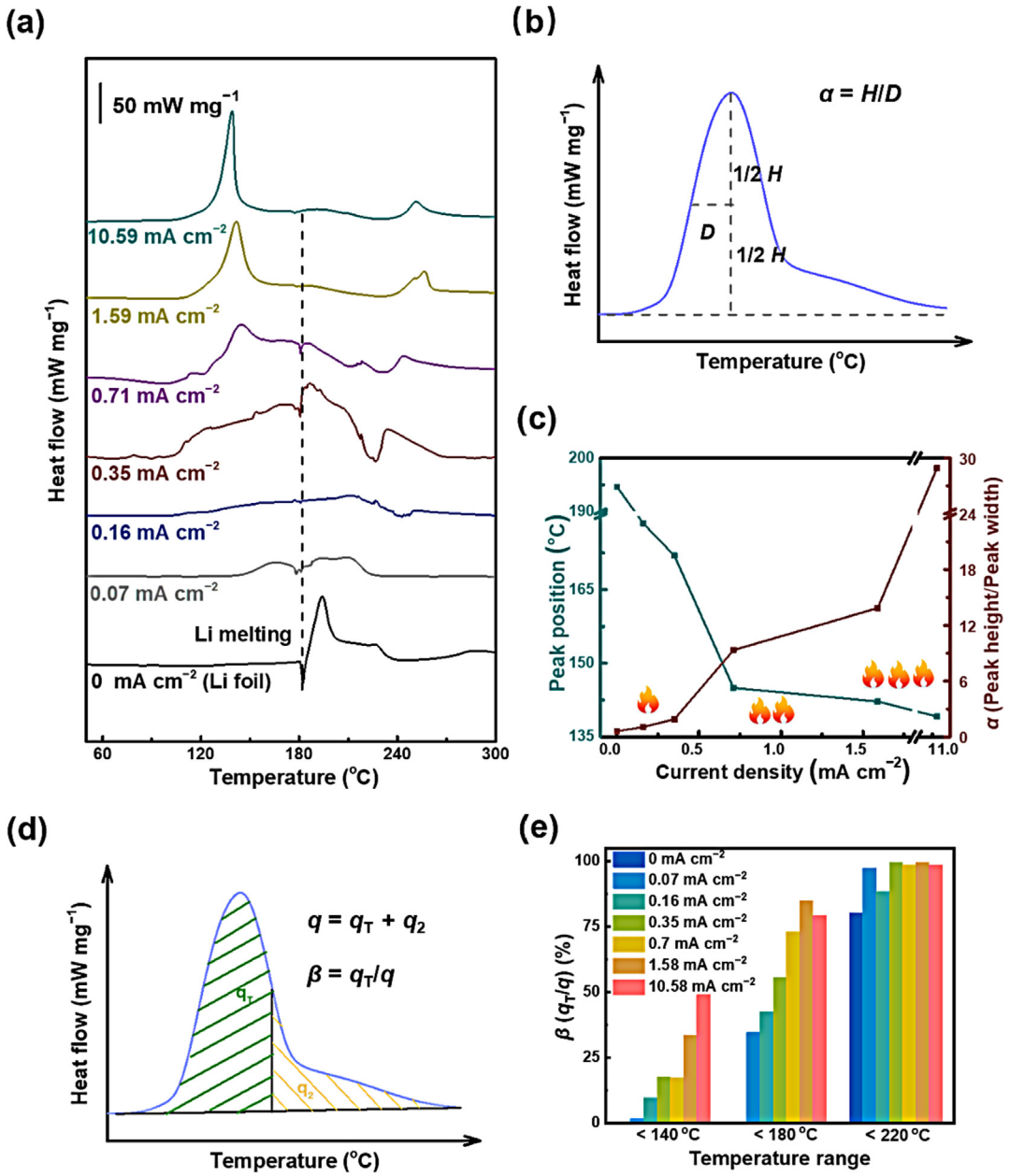

Fig. 3. Thermal stability of Li deposits with different specific surface area against $LiPF_6$-EC/DEC electrolyte. (a) DSC results for the electrolyte and Li metal obtained at different current densities. (b) The illustration of peak height and peak width obtained from DSC tests. The peak height is obtained at maximum heat flow and the peak width is defined at half maximum heat flow in the raising side. (c) Left panel: the relationship between depositing current density and the peak position of maximum heat flow; Right panel: α before 180 °C vs. deposition current density. (d) The schematic diagram of q_T and q. q_T is defined as the released heat from 30 to T °C and q is total heat release from 30 to 300 °C. (e) β for the reaction between Li deposits and electrolyte. All the mass in the whole article during DSC tests is based on the metallic Li.

columnar Li is calculated according to the Li mass on the Cu electrode and the corresponding diameters of the Li columns (Fig. S8). The results reveal that the specific surface area of columnar Li increases from 5.0 to 49.5 $m^2\ g^{-1}$ as the current density rises from 0.07 to 1.59 mA cm^{-2} (Fig. 2c and Table S1). Therefore, dendritic Li is easily occurred with a large specific surface area at a high plating current density.

3.3. Thermal stability of Li deposits against $LiPF_6$-EC/DEC electrolyte

DSC was used to characterize the thermal stability between Li metal with different specfic surface areas and $LiPF_6$-EC/DEC electrolyte (Fig. 3). The effect of prisitine SEI on DSC curves is excluded (Fig. S9). The exothermic peaks in Fig. 3(a) can be attributed to the reaction between Li metal and $LiPF_6$-EC/DEC electrolyte. Fresh Li foil is stable with electrolyte until the melting point of Li metal due to the significant increase in specific surface area after 180 °C. The location of the first exothermic peak begins to move towards lower temperature to 178, 171, 144, 142, and 139 °C with the increasing of current density to 0.16, 0.35, 0.71, 1.59, and 10.59 mA cm^{-2} respectively (Fig. 3c and Table S2). With the rise of the specific surface area of Li deposits, the chemical reaction between Li metal and elelctrolyte aggravates at lower temperature, implying the negative effect of dendritic Li on the thermal safety of LMBs compared to homogeneous Li deposition.

In addition to the positions of the exothermic peaks, the ratio (α) between peak height (H) and peak width (D) (Fig. 3b) is adopted to indicate the speed of heat release, and the ratio (β) between the

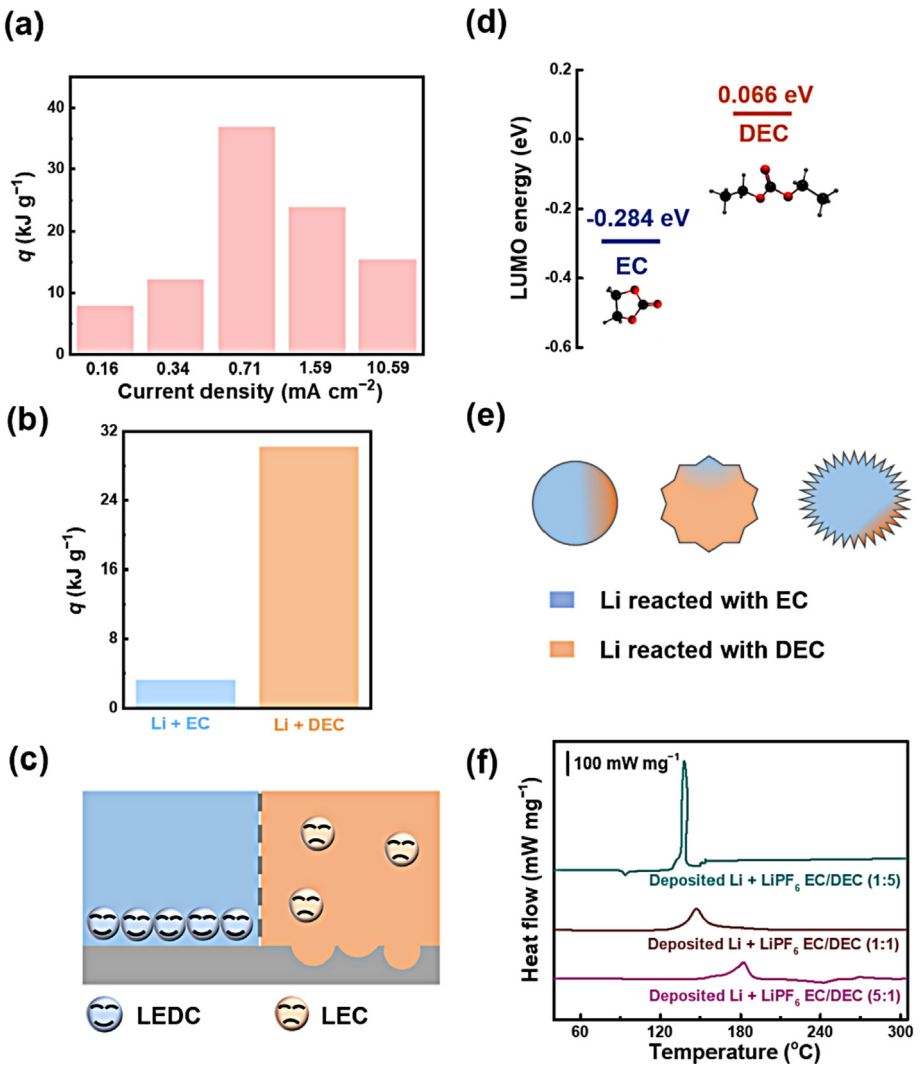

Fig. 4. Heat releasing behaviours depending on the solvent ratios. (a) Heat release per gram Li with $LiPF_6$-EC/DEC electrolyte. (b) The different heat releases for the reaction of Li + DEC and Li + EC. (c) Scheme of interface formation by the reaction products in different solvents. (d) The comparison of LUMO energies between EC and DEC solvents. Hydrogen, carbon, and oxygen atoms are marked with white, grey, and red, respectively. The cyan and yellow regions represent the positive and negative parts of LUMOs, respectively (isovalue: 0.02). (e) The scheme of Li deposits with different specific surface areas consumed in $LiPF_6$-EC/DEC electrolyte. The Li deposits with moderate specific surface area are mostly consumed by DEC while the Li deposits with really the low or relatively high specific surface area are mostly consumed by EC. (f) DSC traces of Li deposited at 10.59 mA cm^{-2} with electrolytes containing different volume ratios of EC and DEC.

heat release in different temperature ranges (q_T) and the total heat release (q) (Fig. 3d) represents the dangerous level of the reaction between Li deposits and electrolyte correspondingly. As shown in Fig. 3(c), α is positively related to current density. The α is 0.45 and 28.33 for Li deposited at 0.16 and 10.59 mA cm^{-2}, respectively. The β changes with the current density at different temperature ranges. In detail, β is 9.65%, 17.42%, 17.28%, 33.46%, and 48.87% for Li deposited at 0.16, 0.35, 0.71, 1.59, and 10.59 mA cm^{-2}, respectively, in the temperature range from 30 to 140 °C, indicating that highly dendritic Li can react with electrolyte and generate large heat at low temperature (Table S2). As a result, it demonstrates the positive relationship between the specific surface area and the exothermic reaction. The formation of highly dendritic Li during the repeated plating and stripping has an obviously adverse role in the safety of LMBs.

It is widely accepted that thermal runaway is attributed to the mismatch between heat production and dissipation in a working cell. Therefore, the heat release of per gram Li obtained at different current densities with $LiPF_6$-EC/DEC electrolyte is calculated and regarded as one of the important indicators for the safety of LMBs (Table S2). The metallic Li deposited on the Cu plate was tested with gas chromatographic (GC) (Fig. S2) and the Li metal is completely consumed by electrolyte, indicated by the disappearance of the exothermic peak of Li solidification during the cooling process of samples (Fig. S10). The relationship between heat release per gram Li and current densities indicates a volcano-shaped trend (Fig. 4a). The thermal stability of Li metal with different electrolyte components including DEC, EC solvents, and $LiPF_6$ salt was investigated (Fig. S11).

Firstly, there is only an endothermic peak (180 °C) in Fig. S11(a), displaying the high thermal stability between Li metal and $LiPF_6$. In addition, the content of Li metal reacting with solvents should be determined with the aim to calculate the heat release per gram Li metal with DEC or EC solvents. As shown in Fig. S11(b), the endothermic peak at 180 °C of Li metal melting cannot be observed, indicating the complete consumption of Li foil by DEC. Similarly, no Li solidification peaks take place during the cooling process which implies the complete reaction of Li deposits by EC as well (Fig. S11c). In addition, the endothermic peaks of DEC and EC evaporation are far from the exothermic peaks resulting

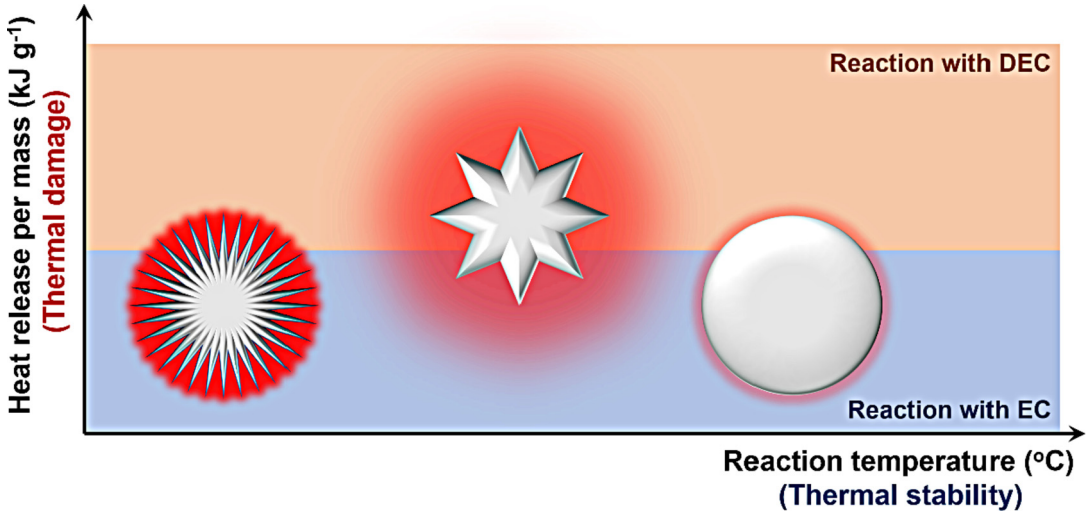

Fig. 5. The reaction between Li deposits with different specific surface area and 1.0 M $LiPF_6$-EC/DEC electrolyte. The reaction temperature between Li metal and electrolyte deviates to a lower temperature with the increase of the specific surface areas of Li metal. In comparison, the heat release of per gram Li increases firstly and then decreases with the increase in the specific surface areas of Li metal.

from the reaction between Li foils and DEC, and Li deposits and EC respectively, hence, the influence of evaporation of solvents on heat release of the reactions can be ignored. The heat generation (q) is about 10 times greater for Li + DEC (30.2 kJ g^{-1}) than that of Li metal with EC (3.2 kJ g^{-1}) (Fig. 4b). Therefore, the different amounts of heat release for the reaction between Li deposits and electrolytes can be attributed to the different ratios of Li metal reacting with DEC or EC. The mass percent of moderately dendritic Li reacting with DEC is thought to be higher than that of Li foil and dendritic Li with large specific surface areas. The different reaction mechanisms can be illustrated in the following analysis: (1) Compared to EC, DEC can react with Li metal of all specific surface areas, even the fresh Li foil at room temperature [63]. It is due to the highly dispersed feature of the reaction products of Li and DEC, while the reaction products between EC and Li metal have a poor dispersibility in the electrolyte and the reactions are self-limited (Fig. 4c). Consequently, Li foil tends to react with DEC rather than EC at temperature below 180 °C. However, the limitation of lithium ethylene dicarbonate (LEDC) is weakened when Li metal is highly dendritic or molten. (2) The lowest unoccupied molecular orbital (LUMO) of EC is lower than that of DEC (Fig. 4d). The electrons are easy to transfer from metallic Li to EC, indicating that Li metal tends to thermodynamically react with EC [64]. Based on the above analysis, highly dendritic Li (such as 49.5 m^2 g^{-1} dendrite) and Li foil react mostly after 180 °C without the protective of LEDC. The mass percent of them, reacting with EC, is higher than that of moderately dendritic Li (Fig. 4e). Due to the different amounts of heat release and reaction kinetics between Li metal and different solvents, the thermal safety of LMBs can be regulated by the ratio of the different solvents. Li metal obtained at 10.59 mA cm^{-2} is utilized to react with the electrolyte containing different volume ratios of EC and DEC (from 0.2 to 5) (Fig. 4f). A stronger exothermic peak is aroused as long as the electrolyte contains a larger DEC ratio, which is attributed to the huge difference in heat release of Li reacting with EC or DEC. It should be noted that the exothermic reaction between Li deposits and electrolyte (1.0 M $LiPF_6$-EC/DEC (1:5 by vol.)) is overheated, because the tremendous heat release rate is much higher than the set temperature rises rate of DSC (10 °C min^{-1}), leading to the uncontrollable temperature rise for sample. In addition, due to the protective role of LEDC, the exothermic peak shifts to a higher temperature with the increasing of volume ratios of EC in ester electrolyte. Therefore, the composition of the electrolyte obviously affects the exothermic behavior between Li metal and electrolytes. The safety performance of LMBs is not only strongly dependent on the structure of the Li metal anode, but also on the ratio of different solvents.

Based on the above disscussion, the relationship between the Li deposits with different specific surface areas and the thermal safety of LMBs is closely correlated (Fig. 5). (1) The reaction temperature decreases with the increase in the specific surface area of Li metal, indicating the increase of the thermal runaway risks with the pulverization of Li anode. (2) The total heat release per gram Li with electrolytes increases firstly and then decreases with the increase in the specific surface areas of Li metal, which results from the different ratios of Li metal reacting with DEC or EC. The more metal Li reacts with DEC, the greater the total heat release.

4. Conclusions

The thermal safety of LMBs is inversely proportional to the specific surface area of Li metal anode, which is demonstrated by ARC results from the cell level and the features of DSC curves from the material level. During the ARC tests, compared to LMB with Li deposits (T_1: 41.9 °C, T_2: 111 °C), LMB with fresh Li foil indicates higher T_1 (68.5 °C) and T_2 (211 °C), confirming that the increasing specific surface area of Li anode reduces the thermal safety of LMB. In addition, the initial exothermic temperature of Li metal and electrolyte from the DSC results is 194 °C for fresh Li foil and 142 °C for 49.5 m^2 g^{-1} dendrite. Additionally, the heat release of the reaction between Li metal and DEC solvent is several-fold relative to that of Li metal with EC solvent. More importantly, Li deposits with different specific surface areas can regulate the electrochemical routes: The mass percent of Li foil and 49.46 m^2 g^{-1} dendrite reacting with EC is higher than that of moderately dendritic Li. Therefore, the electrolyte composition can significantly modulate the heat output during thermal runaway. These results present the exothermic reaction scenarios of dendritic Li with different specific surface areas and electrolytes with various solvent ratios, which affords fresh insights into the thermal stablity of Li metal anode and emerging concept to achive safe LMBs.

Declaration of competing interest

We declare that we have no financial and personal relationships with other people or organizations that can inappropriately influence the manuscript.

Acknowledgments

This work was supported by the National Key Research and Development Program (2021YFB2500300), the National Natural Science Foundation of China (22179070, 22109084, 22075029, and U1932220), the China Postdoctoral Science Foundation (2021TQ0161 and 2021M691709), and the Beijing Natural Science Foundation (JQ20004).

Appendix A. Supplementary data

Supplementary data to this article can be found online at https://doi.org/10.1016/j.jechem.2022.05.005.

References

[1] X.B. Cheng, H. Liu, H. Yuan, H.J. Peng, C. Tang, J.Q. Huang, Q. Zhang, SusMat. 1 (2021) 38–50.
[2] X. Xu, Y. Li, J. Cheng, G. Hou, X. Nie, Q. Ai, L. Dai, J. Feng, L. Ci, J. Energy Chem. 41 (2020) 73–78.
[3] Y. Yun, B. Xi, Y. Gu, F. Tian, W. Chen, J. Feng, Y. Qian, S. Xiong, J. Energy Chem. 66 (2022) 339–347.
[4] X. Shen, X.-Q. Zhang, F. Ding, J.-Q. Huang, R. Xu, X. Chen, C. Yan, F.-Y. Su, C.-M. Chen, X. Liu, Q. Zhang, Energy Mater. Adv. 2021 (2021) 1205324.
[5] H. Liu, X. Cheng, Y. Chong, H. Yuan, J.-Q. Huang, Q. Zhang, Particuology 57 (2021) 56–71.
[6] J. Liu, H. Yuan, X. Tao, Y. Liang, S.J. Yang, J.Q. Huang, T.Q. Yuan, M.M. Titirici, Q. Zhang, EcoMat. 2 (2020) e12019.
[7] X. Wu, K. Chen, Z. Yao, J. Hu, M. Huang, J. Meng, S. Ma, T. Wu, Y. Cui, C. Li, J. Power Sources 501 (2021) 229946.
[8] J. Zhang, H. Wu, B. Tang, T. Liu, S. Tian, L. Zhou, H. Zhang, B. Zhang, J. Zhang, G. Cui, J. Electrochem. Soc. 168 (2021) 60540.
[9] Z. Geng, J. Lu, Q. Li, J. Qiu, Y. Wang, J. Peng, J. Huang, W. Li, X. Yu, H. Li, Energy Storage Mater. 23 (2019) 646–652.
[10] J. Ding, R. Xu, C. Yan, Y. Xiao, Y. Liang, H. Yuan, J. Huang, Chin. Chem. Lett. 31 (2020) 2339–2342.
[11] J. He, H. Wang, Q. Zhou, S. Qi, M. Wu, F. Li, W. Hu, J. Ma, Small Methods 5 (2021) 2100441.
[12] H. Liu, T. Li, X. Xu, P. Shi, X. Zhang, R. Xu, X. Cheng, J. Huang, Chin. J. Chem. Eng. 37 (2021) 152–158.
[13] X. Chen, M. Shang, J. Niu, ACS Appl. Mater. Interfaces 13 (2021) 34064–34073.
[14] C. Jin, T. Liu, O. Sheng, M. Li, T. Liu, Y. Yuan, J. Nai, Z. Ju, W. Zhang, Y. Liu, Y. Wang, Z. Lin, J. Lu, X. Tao, Nat. Energy 6 (2021) 378–387.
[15] X.-Q. Xu, F.-N. Jiang, S.-J. Yang, Y. Xiao, H. Liu, F. Liu, L. Liu, X.-B. Cheng, J. Energy Chem. 69 (2022) 205–210.
[16] S.-J. Tan, J. Yue, Y.-F. Tian, Q. Ma, J. Wan, Y. Xiao, J. Zhang, Y.-X. Yin, R. Wen, S. Xin, Y.-G. Guo, Energy Storage Mater. 39 (2021) 186–193.
[17] Y. Lu, C.Z. Zhao, H. Yuan, X.B. Cheng, J.Q. Huang, Q. Zhang, Adv. Funct. Mater. 31 (2021) 2009925.
[18] O. Sheng, H. Hu, T. Liu, Z. Ju, G. Lu, Y. Liu, J. Nai, Y. Wang, W. Zhang, X. Tao, Adv. Funct. Mater. 32 (2021) 2111026.
[19] Y. Ouyang, W. Zong, J. Wang, Z. Xu, L. Mo, F. Lai, Z.-L. Xu, Y.-E. Miao, T. Liu, Energy Storage Mater. 42 (2021) 68–77.
[20] S.-J. Yang, X. Shen, X.-B. Cheng, F.-N. Jiang, R. Zhang, H. Liu, L. Liu, H. Yuan, J. Energy Chem. 69 (2022) 70–75.
[21] S. Zhang, W. Deng, X. Zhou, B. He, J. Liang, F. Zhao, Q. Guo, Z. Liu, Mater. Today, Energy 21 (2021) 100770.
[22] R. Chen, A.M. Nolan, J. Lu, J. Wang, X. Yu, Y. Mo, L. Chen, X. Huang, H. Li, Joule 4 (2020) 812–821.
[23] R. Chen, C. Yao, Q. Yang, H. Pan, X. Yu, K. Zhang, H. Li, ACS Appl. Mater. Interfaces 13 (2021) 18743–18749.
[24] X. Huang, J. Xue, M. Xiao, S. Wang, Y. Li, S. Zhang, Y. Meng, Energy Storage Mater. 30 (2020) 87–97.
[25] A. Perea, M. Dontigny, K. Zaghib, J. Power Sources 359 (2017) 182–185.
[26] D. Puthusseri, M. Parmananda, P.P. Mukherjee, V.G. Pol, J. Electrochem. Soc. 167 (2020) 120513.
[27] D. Lin, Y. Liu, Y. Cui, Nat. Nanotechnol. 12 (2017) 194–206.
[28] S.J. Tan, W.P. Wang, Y.F. Tian, S. Xin, Y.G. Guo, Adv. Funct. Mater. 31 (2021) 2105253.
[29] A.M. Beese, D. Mohr, Acta Mater. 59 (2011) 2589–2600.
[30] D. Ren, H. Hsu, R. Li, X. Feng, D. Guo, X. Han, L. Lu, X. He, S. Gao, J. Hou, Y. Li, Y. Wang, M. Ouyang, eTransportation 2 (2019) 100034.
[31] Y. Liu, K. Yang, M. Zhang, S. Li, F. Gao, Q. Duan, J. Sun, Q. Wang, J. Energy Chem. 65 (2022) 532–540.
[32] S. Yuan, C. Chang, S. Yan, P. Zhou, X. Qian, M. Yuan, K. Liu, J. Energy Chem. 62 (2021) 262–280.
[33] Y. Chen, Y. Kang, Y. Zhao, L. Wang, J. Liu, Y. Li, Z. Liang, X. He, X. Li, N. Tavajohi, B. Li, J. Energy Chem. 59 (2021) 83–99.
[34] Z. Wang, J. Yuan, X. Zhu, H. Wang, L. Huang, Y. Wang, S. Xu, J. Energy Chem. 55 (2021) 484–498.
[35] D. Mohr, M. Dunand, K.-H. Kim, Int. J. Plasticity 26 (2010) 939–956.
[36] L. Liu, X. Feng, C. Rahe, W. Li, L. Lu, X. He, D.U. Sauer, M. Ouyang, J. Energy Chem. 61 (2021) 269–280.
[37] Y. Wu, S. Wang, H. Li, L. Chen, F. Wu, InfoMat 3 (2021) 827–853.
[38] Q. Xie, Z. Cui, A. Manthiram, Adv. Mater. 33 (2021) 2100804.
[39] Y. Li, X. Feng, D. Ren, M. Ouyang, L. Lu, X. Han, ACS Appl. Mater. Interfaces 11 (2019) 46839–46850.
[40] M. Yuan, K. Liu, J. Energy Chem. 43 (2020) 58–70.
[41] Q. Zhou, S. Dong, Z. Lv, G. Xu, L. Huang, Q. Wang, Z. Cui, G. Cui, Adv. Energy Mater. 10 (2019) 1903441.
[42] J.-I. Yamaki, Y. Baba, N. Katayama, H. Takatsuji, M. Egashira, S. Okada, J. Power Sources 119–121 (2003) 789–793.
[43] G. Zhang, X. Wei, S. Chen, J. Zhu, G. Han, X. Tang, W. Hua, H. Dai, J. Ye, ACS Appl. Mater. Interfaces 13 (2021) 35054.
[44] C. Fear, M. Parmananda, V. Kabra, R. Carter, C.T. Love, P.P. Mukherjee, Energy Storage Mater. 35 (2021) 500–511.
[45] W. Cai, C. Yan, Y.X. Yao, L. Xu, X.R. Chen, J.Q. Huang, Q. Zhang, Angew. Chem., Int. Ed. 60 (2021) 13007–13012.
[46] J. Liu, Q. Duan, L. Feng, M. Ma, J. Sun, Q. Wang, J. Energy Storage 29 (2020) 101397.
[47] W. Ren, C. Ding, X. Fu, Y. Huang, Energy Storage Mater. 34 (2021) 515–535.
[48] B. Wu, J. Lochala, T. Taverne, J. Xiao, Nano Energy 40 (2017) 34–41.
[49] H. Lee, X. Ren, C. Niu, L. Yu, M.H. Engelhard, I. Cho, M.H. Ryou, H.S. Jin, H.T. Kim, J. Liu, W. Xu, J.G. Zhang, Adv. Funct. Mater. 27 (2017) 1704391.
[50] M. Ye, Y. Xiao, Z. Cheng, L. Cui, L. Jiang, L. Qu, Nano Energy 49 (2018) 403–410.
[51] Y. Yuan, F. Wu, Y. Bai, Y. Li, G. Chen, Z. Wang, C. Wu, Energy Storage Mater. 16 (2019) 411–418.
[52] H. Liu, X. Cheng, R. Zhang, P. Shi, X. Shen, X. Chen, T. Li, J. Huang, Q. Zhang, Trans. Tianjin Univ. 26 (2020) 127–134.
[53] Y.Y. Hu, R.X. Han, L. Mei, J.L. Liu, J.C. Sun, K. Yang, J.W. Zhao, Mater. Today, Energy 19 (2021) 100608.
[54] C. Fang, J. Li, M. Zhang, Y. Zhang, F. Yang, J.Z. Lee, M.H. Lee, J. Alvarado, M.A. Schroeder, Y. Yang, B. Lu, N. Williams, M. Ceja, L. Yang, M. Cai, J. Gu, K. Xu, X. Wang, Y.S. Meng, Nature 572 (2019) 511–515.
[55] K. Raghavachari, Theor. Chem. Acc. 103 (2000) 361–363.
[56] A.V. Marenich, C.J. Cramer, D.G. Truhlar, J. Phys. Chem. B 113 (2009) 6378–6396.
[57] Q.-K. Zhang, X.-Q. Zhang, H. Yuan, J.-Q. Huang, Small Science 1 (2021) 2100058.
[58] Y. Fernandes, A. Bry, S. de Persis, J. Power Sources 389 (2018) 106–119.
[59] N.E. Galushkin, N.N. Yazvinskaya, D.N. Galushkin, J. Electrochem. Soc. 166 (2019) A897–A908.
[60] S. Yang, X. Xu, X. Cheng, X. Wang, J. Chen, Y. Xiao, H. Yuan, H. Liu, A. Chen, W. Zhu, J. Huang, Q. Zhang, Acta Phys. Chim. Sin. 37 (2021) 2007058.
[61] A. Pei, G. Zheng, F. Shi, Y. Li, Y. Cui, Nano Lett. 17 (2017) 1132–1139.
[62] Y. Xu, H. Wu, H. Jia, J.G. Zhang, W. Xu, C. Wang, ACS Nano 14 (2020) 8766–8775.
[63] S.-J. Yang, N. Yao, X.-Q. Xu, F.-N. Jiang, X. Chen, H. Liu, H. Yuan, J.-Q. Huang, X.-B. Cheng, J. Mater. Chem. A 9 (2021) 19664–19668.
[64] G. Xu, C. Pang, B. Chen, J. Ma, X. Wang, J. Chai, Q. Wang, W. An, X. Zhou, G. Cui, L. Chen, Adv. Energy Mater. 8 (2018) 1701398.